

Simulation design of online Beam Monitoring for the MULTISCAN 3D Laser-Plasma X-Ray Source

Eric Garrido^{1,*}, David Tisseur², Cedric Carasco¹ and Bertrand Perot¹

¹ CEA, DES, IRESNE, DTN, SMTA, Nuclear Measurement Laboratory, France

² CEA, DES, IRESNE, DER, SPESI, Dosimetry, Sensors and Instrumentation Laboratory, France

(*) eric.garrido2@cea.fr

Abstract— Many private and public actors in the security field use imaging systems with embedded X-ray accelerators for rail, seaports and border controls. These accelerators produce X-rays by the Bremsstrahlung effect, leading the output beam to have a very wide energy spectrum which precise form is difficult to know, especially the end-point energy. Mastering this energy distribution is nevertheless essential for certain applications like material discrimination. In addition, fluctuations over time or even from one pulse to another can disturb the analysis of the images and it is expected that the new X-ray sources based on laser-plasma accelerators, which are developed in the frame of MULTISCAN 3D H2020 project, will also increase this beam instability. In this context, we study a direct beam measurement at the exit of the target with a minimum footprint and a fast response, so that the results can be used in real time. A 50 mm × 50 mm × 2 mm scintillator is irradiated on the side by the X-ray beam (i.e. on a 50 mm × 2 mm face) and filmed from the top (i.e. on a 50 mm × 50 mm face). The light intensity of the image obtained by the camera is directly proportional to the dose deposition in this scintillator, and the depth profile is related to the X-ray energy spectrum. A study on different materials (PVT, CsI, BGO) is presented in order to determine the optimal scintillator. Several unfolding algorithms are examined to reconstruct the X-ray spectrum from monochromatic response functions of these detectors, which are calculated using MCNP code for a range of photon energies covering the expected X-ray spectrum. This study based on simulation results shows the feasibility of this technique, it appears that the Sequential Least Squares Programming (SLSQP) minimization algorithm gives the most promising results and that the CsI scintillator provides better spectral information. It is probably due to the intermediate dose profile shape between PVT (flat falling tail) and BGO (steep rise). The binning of the depth profile (typically 100 μm or less) is also an important parameter to describe the initial steep march, and thus to keep the spectral information therein.

Keywords —Laser-plasma, X-ray source, monitoring, scintillator.

I. INTRODUCTION

ALTHOUGH commonly used in the security field, the energy spectrum of the X-ray beams are generally not fully mastered, both in intensity and in energy spectrum, especially

the end-point energy. The current method used to evaluate their energy spectrum consists of performing several transmission measurements with increasing thicknesses of material plates, like aluminum, inserted between the accelerator and the detection system [1,2]. The transmitted signal, as a function of aluminum thickness, is unfolded to obtain the beam spectrum, see Fig. 1. However, this method requires a specific setup, is time-consuming, and therefore does not allow pulse-to-pulse online monitoring during the inspection.

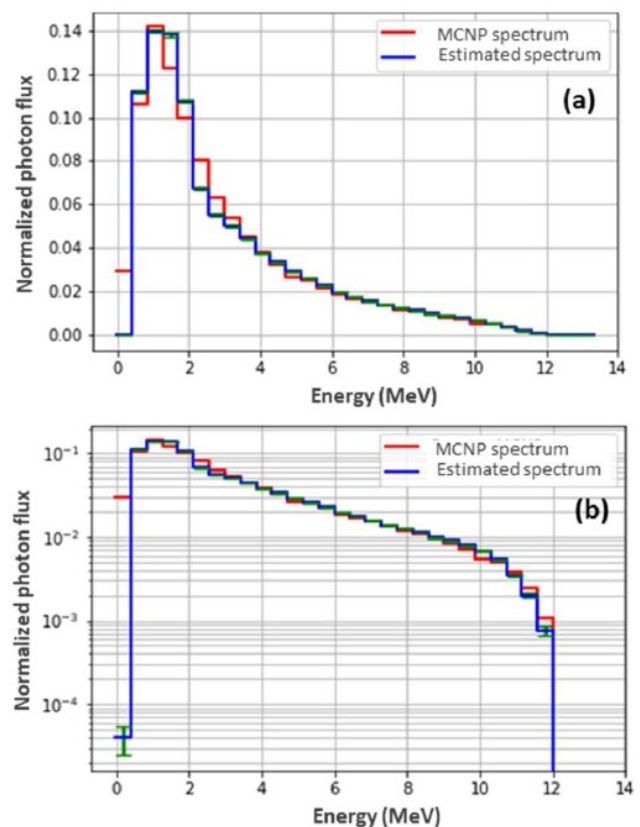


Fig. 1. Typical bremsstrahlung X-ray spectrum produced by a 12 MeV electron LINAC (linear accelerator), calculated with MCNP and estimated with the method using increasing aluminium plates [2]. (a) Spectrum in linear scale, and (b) in semi-logarithmic scale.

Having a non-invasive and instantaneous measurement would permit real-time monitoring of beam shape and intensity, allowing an adjustment or adaptation of the imaging algorithms to obtain more accurate results.

The solution studied in this work consists in measuring with

a camera the light emitted by a thin scintillation plate crossed by the incident beam on one of its small faces. Therefore, it makes it possible to perform a beam characterization in a single acquisition with a minimum footprint. This requires the thin crystal plate to be long enough for a sufficient dose deposition, and a scintillation material with a good light yield at the proper wavelength for the camera. The first part of this article describes the proposed setup.

The second part of this study concerns the development of the analysis code that allows, from dose deposition data, to retrieve the X-ray spectrum distribution. To this aim, we calculate a database of dose-deposition response functions for mono-energy photons covering the range of the X-ray beam spectrum, and for the different scintillation materials, using MCNP 6.1 Monte Carlo computer code [3]. Then, we study different unfolding algorithms to reconstruct the X-ray beam spectrum from a linear combination of these response functions, and we compare the results for the different scintillators.

II. MEASUREMENT PRINCIPLE

As mentioned in the introduction, this method utilizes the thickness of a scintillating crystal to observe the deposition within its depth, following the setup described in [1] and schematized in Fig. 2. An example of image acquisition is shown in Fig. 3 and the associated dose profile in Fig. 4. This measurement offers spectral information similar to multiple acquisitions with increasing material thicknesses between the beam and detector, but in a single acquisition, enabling real-time monitoring.

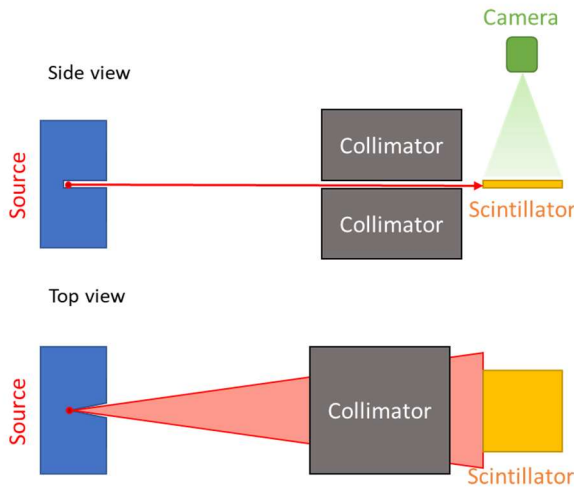


Fig 2: Set-up of the 50 mm × 50 mm × 2 mm scintillator and the camera with respect to the X-ray beam.

The poly-energetic spectrum of the X-ray beam can be discretized into a sum of mono-energetic beams, as shown in Fig. 5. Note that increasing the number of channels would improve the characterization of the X-ray spectrum, as can be seen at the low energies in Fig. 5. We consider that the dose deposition in the scintillation plate resulting from this poly-energetic spectrum is a weighted sum of the dose depositions from each of these mono-energetic beams, as formalized by equation (1):

$$D = \sum_i P_i \cdot D_i \quad (1)$$

where D is the total dose deposition profile (Fig. 4), P_i is the weighting of the mono-energy contribution i in the poly-energetic spectrum, and D_i is the dose deposition profile of energy i (see Fig. 5, bottom panel).

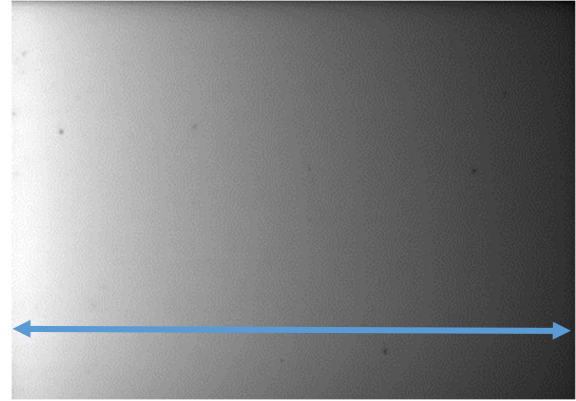


Fig. 3: Example of a dose deposition image in a CsI scintillator irradiated by the bremsstrahlung X-ray beam of a 9 MeV electron LINAC simulated with MCNP 6.1. The line with the double arrow indicates the axis for the associated dose profile shown on Fig. 4.

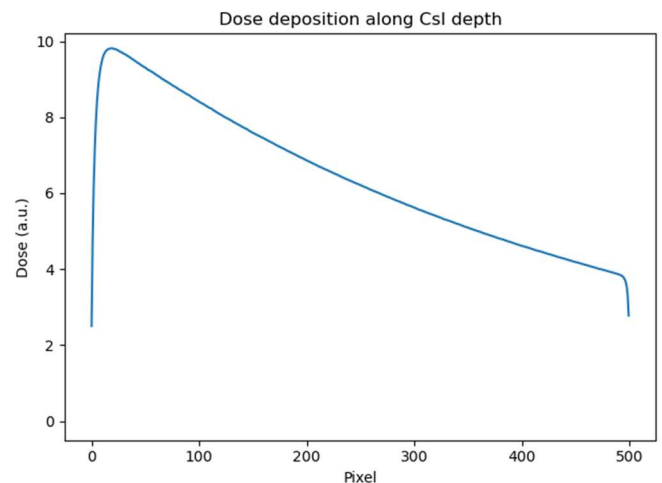


Fig 4: Dose profile along the blue arrow axis on the Fig. 3.

By knowing the dose deposition profiles of each mono-energetic contribution (database of response functions), we can determine their respective weights by minimizing the difference between the total measured dose and the dose resulting from their weighted sum. We thus obtain a spectral characterisation of the poly-energetic beam.

III. UNFOLDING ALGORITHM

We first build a database of dose deposition profiles in the three 50 mm × 50 mm × 2 mm scintillation plates (CsI, BGO, PVT) for mono-energetic photons covering the expected 0-10 MeV range of the X-ray beam, using MCNP 6.1 simulations. To remain consistent with the experiment described in reference [1], the pixels of the camera and of the simulated dose profiles have a size of 100 μm. This parameter and its associated limitations will be discussed later.

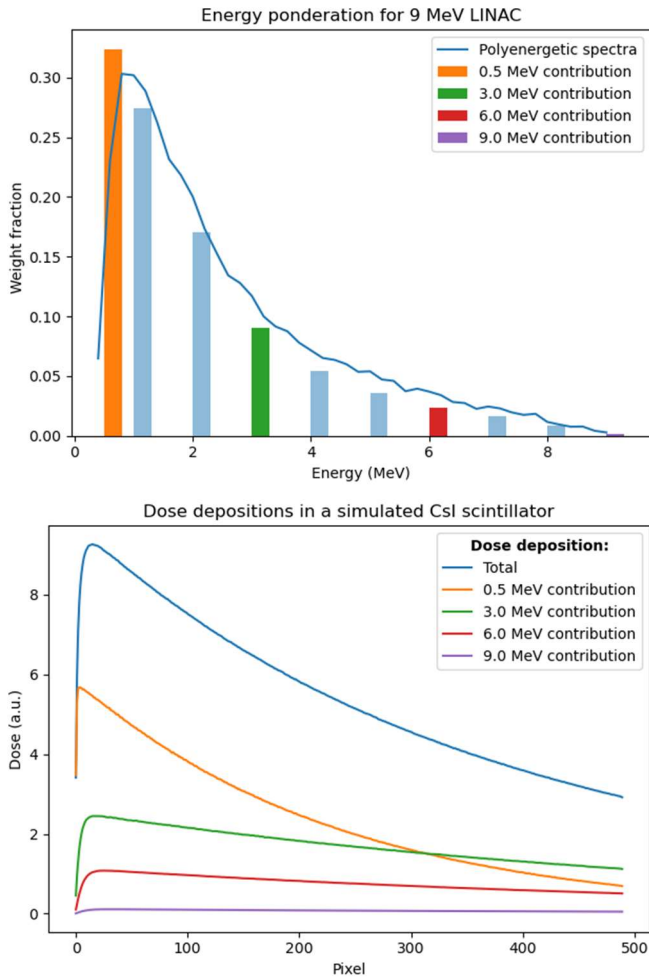


Fig. 5: Segmentation of a poly-energetic spectrum into a histogram of 10 mono-energetic contributions (top picture). Dose deposition profile simulated on a CsI scintillator for the poly-energetic spectrum, and a few examples of dose profiles for mono-energy photons (bottom picture).

An example for the simulation results is given in Fig. 6 for the CsI detector. The MCNP model reproduces an X-ray fan beam impinging a 50 mm × 50 mm × 2 mm scintillator irradiated on one of its thin faces (i.e. a 50 mm × 2 mm side) by a monochromatic photon source from 500 keV to 10 MeV.

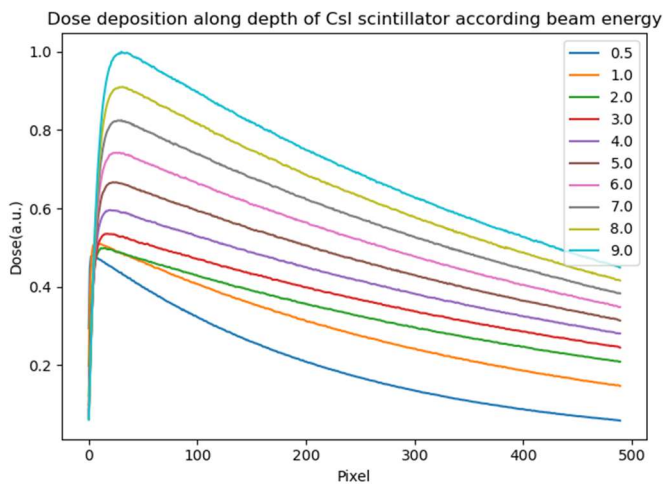


Fig. 6 : Dose deposition profiles in the CsI scintillator for single-energy photons

Fig. 7 compares the dose deposition profiles in PVT, CsI and BGO scintillators for the 1 MeV and 6 MeV beams, showing differences caused by their respective atomic numbers and densities listed in Table I. A high density and high atomic number material like BGO (7.13 g.cm^{-3} , $\text{Bi}_4\text{Ge}_3\text{O}_{12}$ - $Z_{\text{eff}} = 74$) exhibits a sharp, decreasing exponential profile, while the low density and low atomic number PVT (1.05 g.cm^{-3} , $[\text{CH}_2\text{-CH-CH}_3]_n$ - $Z_{\text{eff}} = 5.6$) shows a slow linear decay. CsI with a 4.51 g.cm^{-3} density and Z_{eff} of 54 appears to be intermediate. It is also important to note that the deformation of the dose deposition as a function of energy becomes more significant with the increase of the density and atomic number of the scintillator as the comparison of the top and bottom figures on Fig. 7 depicts that.

TABLE I
 CHARACTERISTICS OF SCINTILLATOR MATERIALS

Material	Density (g.cm^{-3})	Z_{eff}	Maximum wavelength	Light-yield (photons/keV)
PVT	1.05	5.6	423 nm	10
CsI	4.51	54	550 nm	60
BGO	7.13	74	480 nm	8.5

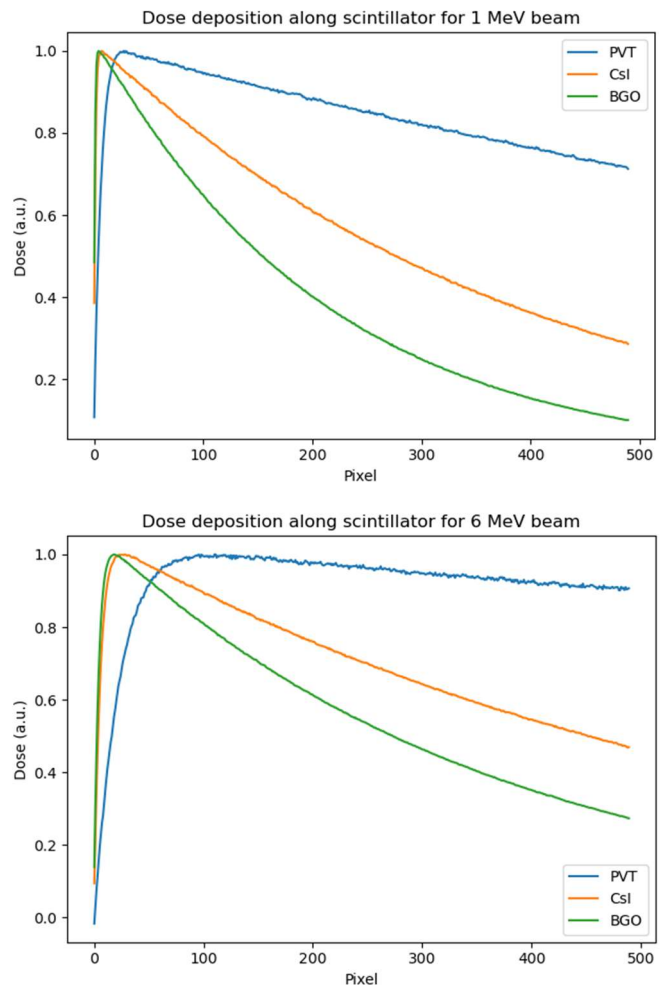


Fig. 7 : Dose depositions in different scintillators obtained from simulations at energies of 1 MeV (top picture) and 6 MeV (bottom picture).

The unfolding consists in determining the weights of each mono-energetic contribution that best approximates the dose deposition obtained with the poly-energetic beam. For each iteration where the algorithm generates a new weights vector for the mono-energetic contributions, it calculates the residual distance, or second-order norm ($norm_{L2}$), along all depth pixels j between the actual dose d and the reconstructed dose d' , as described below:

$$norm_{L2} = [\sum_j (d_j - d'_j)^2]^{1/2} \quad (2)$$

We opted for a turnkey code that enabled us to obtain a quick response. Therefore, we chose the SciPy suite [3], which allows to test different minimization methods. This library, simple and quick to implement, required only a few parameters as input such as the minimization function equation (2), its tolerance and the maximum number of iterations. We have defined constraints on the output X-ray spectrum, which follows the well-known bremsstrahlung spectrum shape with a maximum intensity at low energy, and the fact that no mono-energetic contribution can be negative.

A minimization method need to be selected, we decide to chose one of those implemented by default in the SciPy library: Nelder-Mead, Powell, CG, BFGS, L-BFGS-B, TNC, COBYLA, SLSQP, and trust-constr. In order to determine the most suitable one, we compare all of these methods for the three tested scintillators, and Table II reports the obtained residual distance described in equation (2). It appears that the SLSQP method stands out from the others with lower values (below 0.1) for all three scintillators. We can add that CsI and BGO dose profiles are better fitted than that of PVT.

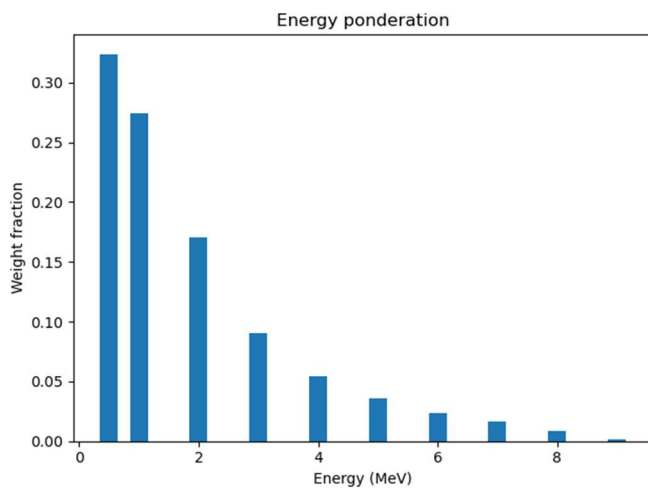


Fig 8: Resampling on 10 energy channels of the spectrum shown in Fig. 5.

Fig. 9 presents the SLSQP results (fit of the dose profile resulting from the unfolding) for each scintillator. The bottom plot focusses on the first 5 mm of the scintillator, showing that the number of pixels in the rising part, up to the dose peak, is quite limited. Therefore, thinner pixels than those of the camera (100 μm as in [1]) are necessary to describe this steep rise with a sufficient number of samples, especially for the CsI and BGO scintillators. This is confirmed by other studies (not reported

here) showing that using pixels down to 10 μm significantly improves the fitting results for high-density scintillators.

TABLE III
RESIDUAL DISTANCE BETWEEN THE MEASURED AND THE FITTED DOSE DEPOSITION PROFILES

Method	PVT	CsI	BGO
Nelder-Mead	3.468	2.687	8.851
Powell	1.256	1.107	0.405
CG	4.643	1.396	0.492
BFGS	10.42	24.71	10.88
L-BFGS-B	7.723	0.864	0.421
TNC	0.689	0.282	0.203
COBYLA	1.470	7.154	2.856
SLSQP	0.044	0.007	0.016
trust-constr	4.224	0.670	0.322

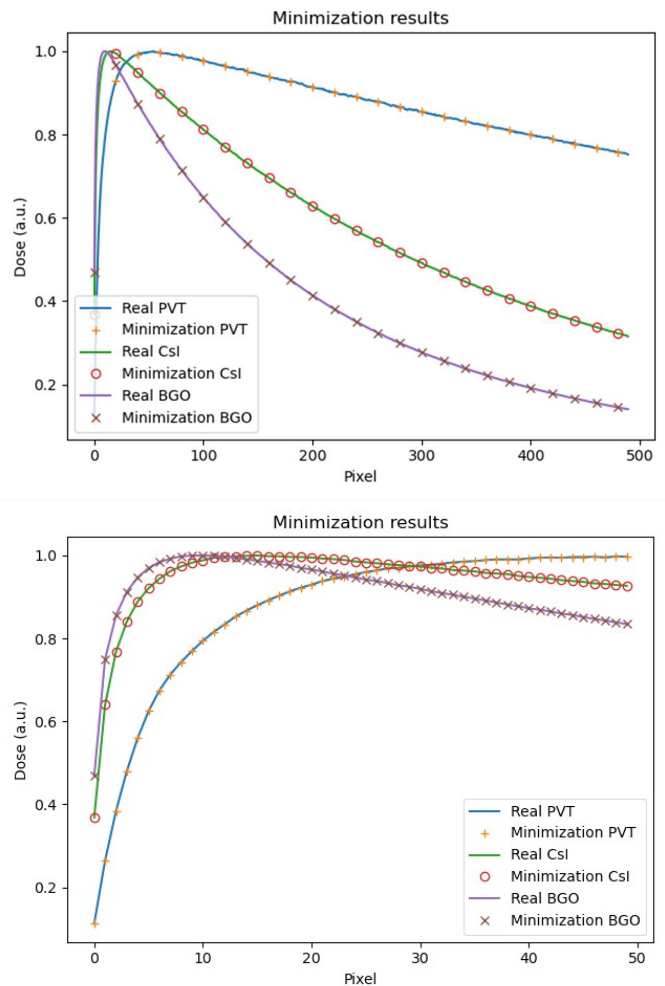


Fig. 9: Results of the minimization obtained with the SLSQP method for each of the tested scintillators (only 1 result point out of 20 on the whole depth of the scintillator (top) and focussed on the 50 first pixels (up to 5 mm depth) with all the results points (bottom).

Finally, we can globally observe a satisfactory agreement in Fig. 10 between the original X-ray spectrum (“Real”) and the result of the algorithm, which is also described by the residual distance in Table III.

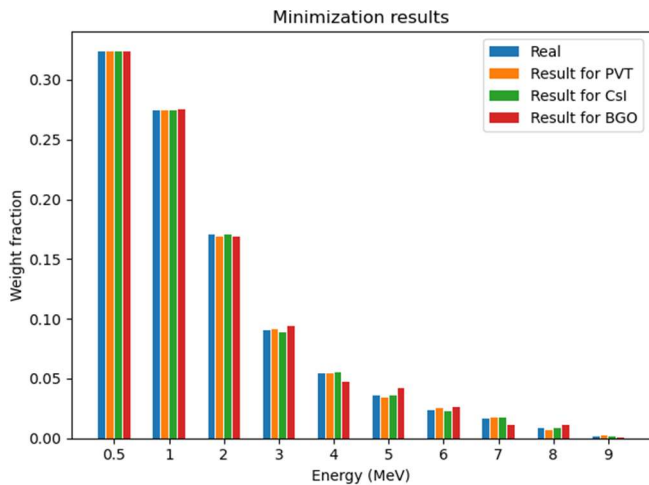


Fig 10: Comparison of the final weights calculated by the minimization code using the SLSQP method for each of the tested scintillators.

TABLE III

RESIDUAL DISTANCE BETWEEN THE REAL AND THE UNFOLDED SPECTRA			
Method	PVT	CsI	BGO
SLSQP	4.233e-3	2.862e-3	1.189e-2

The best agreement between the real and estimated X-ray spectra is obtained with CsI, as for the fit of the dose deposition profile. However, the spectrum reconstructed with BGO is not as good as that of PVT, probably because of insufficient sampling of the steep rise in the beginning of the dose profile. Due to its low density, low light-yield, and emission wavelength ill-suited for the camera [1], the noise on the PVT dose profile may however lead to a poorer reconstructed spectrum in a pulse-to-pulse analysis. As mentioned earlier, the overall shape of the dose deposition is directly related to the density and average atomic number of the scintillator. We will check in future work our guess that excessively steep rising shapes, for high density scintillators, or excessively flat falling tails, for low density, are not optimal for efficiently performing these types of calculations. Therefore, it is worth exploring the range of intermediate densities and atomic numbers, such as with CsI, by studying new scintillators like CaF_2 (3.18 g.cm^{-3}) or GGAG (6.60 g.cm^{-3}). We will also decrease the pixel size ($< 100 \mu\text{m}$) to achieve a better sampling in the first few mm of the dose deposition profile, especially for high densities materials showing an extremely steep rise.

IV. CONCLUSION AND PERSPECTIVES

In this study, we have demonstrated that it is possible, using a minimization algorithm and data obtained from simulations, to reconstruct the dose deposition profile of an X-ray beam poly-energetic spectrum in PVT, CsI and BGO scintillators, by unfolding it into the dose profiles due to mono-energetic photons. We have also demonstrated that using a thin scintillator plate irradiated on its side, along a large thickness, allows recording enough data points in a single pulse acquisition to perform this type of reconstruction. This study allowed us identifying a specific minimization method (SLSQP) for the dose profile fit. However, the choice of the optimal detector is still open, and we recognize that a finer pixel

size ($< 100 \mu\text{m}$) is necessary to achieve more promising results, especially for materials with higher densities. The presented binning of $100 \mu\text{m}$ did not allow for an accurate reproduction of the dose rise up to its maximum for the BGO. This explain why on our study the CsI with its intermediate density, gives us the best results. On the next step, we will reduce the pixel size ($< 100 \mu\text{m}$) of the dose profiles in the simulation data and we will extend our study to new types of scintillators, such as CaF_2 , LYSO, GGAG and CdWO_4 .

In order to test the unfolding robustness, we will also add noise parameters (based on statistical fluctuations of pulse-by-pulse acquisitions) and increase the number of energy channels. Another important aspect of future investigations involves experimental measurements with the set-up depicted in Fig. 1 at the end of accelerators beamlines. The dose deposition images recorded with the camera placed above PVT, CaF_2 , CsI, BGO and GGAG thin scintillator plates will enable us to compare the experimental and simulated dose profiles, as well as the reconstructed X-ray beam energy spectra. Ultimately, we will optimize and test the capability of the algorithm to reconstruct the X-ray spectra pulse by pulse.

ACKNOWLEDGMENT

This work has received funding from the European Union's Horizon 2020 research and innovation program under grant agreement No 101020100. This text reflects only the author's views and the Commission is not liable for any use that may be made of the information contained therein.

REFERENCES

- [1] N. Estre et al., "Design of a very efficient detector for High Energy Tomography," 2018 IEEE Nuclear Science Symposium and Medical Imaging Conference Proceedings (NSS/MIC), Sydney, NSW, Australia, 2018, pp. 1-3
- [2] M. Maulin et al., "Characterization of the X-ray spectrum of a linear accelerator," EPJ Web conf, Volume 253, 2021.
- [3] Pelowitz, Denise B et al., "MCNP6 User's Manual", Los Alamos, NM, USA 2013
- [4] Pauli Virtanen et al., "SciPy 1.0: Fundamental Algorithms for Scientific Computing in Python." Nature Methods, 2020, pp. 261–272.